JOIV : Int. J. Inform. Visualization, 8(3) - September 2024 1476-1486

INTERNATIONAL JOURNAL ON INFORMATICS VISUALIZATION

journal homepage : www.joiv.org/index.php/joiv

Atomic Structure Simulation and Properties' Prediction using Machine Learning on Neodymium Oxide Nanoparticles Zinc Tellurite Glasses Aided by FTIR and TEM Analysis

S.N. Nazrin [a,*], Halimah Badioze Zaman [b], Neesha Jothi [c], Doha Jouay [d], Badreddine Lahrach [d], M.K. Halimah [e]

[a] *Institute of Informatics and Computing in Energy (IICE), Universiti Tenaga Nasional (UNITEN), Malaysia*
[b] *Tan Sri Leo Moggie Distinguished Chair in Energy Informatics, Institute of Informatics and Computing in Energy (IICE), Universiti Tenaga Nasional (UNITEN), Malaysia*
[c] *Department of Computing, College of Computing and Informatics, Universiti Tenaga Nasional (UNITEN), Malaysia*
[d] *School of Industrial Management, University Mohammed VI Polytechnic, Morocco*
[e] *Universiti Putra Malaysia, Malaysia*

Corresponding author: [*]nazirulnazrin@ymail.com; nazirul.nazrin@uniten.edu.my

***Abstract*— The optical, structural, and physical characteristics of zinc tellurite glasses doped with neodymium oxide nanoparticles, which are produced by the melt-quenching method, were examined in this work. The amorphous character of the glasses was verified by XRD analysis. Using the Pair Distribution Function (PDF) and Monte Carlo simulations and visualisation for precise molecule distribution representation, an intuitive Python interface was created to emphasize these features. The density increased with increasing Nd2O3 concentrations, from 5346 to 5606 kg/cm2. Density data was used to infer the molar volume. The best projected density was achieved by the Gradient Boosting Regressor model, with a R2 of 0.9988 and an RMSE of 0.0032; the best predicted molar volume was achieved by linear regression, with a R2 of 1 and an RMSE of 2.67e-15. These models successfully represent the correlations between dopant concentration and glass properties, advancing our knowledge of the optical properties for further glass technology research.**

***Keywords*— Machine learning; glass; PDF function; Monte carlo; visualisation; energy.**

Manuscript received 15 Feb. 2024; revised 29 Apr. 2024; accepted 18 Aug. 2024. Date of publication 30 Sep. 2024.

I. INTRODUCTION

Glass is a versatile substance with many applications. As can be seen with the unaided eye, windows used in building construction are one of the most amazing and undeniable creations. Globally and effectively, the shift from large scale (conventional glass) to Nano scale (fibre optic) has taken place. It has been noted in science that among all elements, glass is the one that is most amorphous. The lack of crystal properties in glass, and its atomic configurations are also asymmetric and have long distance distributions. The atomic arrangements of the glass network serve as evidence for short-range order [1]. It's inorganic compounds with a partial ionic and covalent bond composition, as well as inorganic and organic compounds, with the ability to create chain structures of covalent bonds inside the structure, bound together by Van der Waals forces, are the two categories of materials used to form glass [2].

The concept of excellent glass is being evaluated deeper, and the materials used are being improved. According to a study by Damas et al. (2012) [3], tellurium oxide (TeO2) can function as a host material in glasses due to its lowest phonon energy below 780 cm^{-1} and the greatest apparent transparency, especially in the near-mid infrared spectral bands. These glasses appear to be superior to quartz, phosphate glasses, or borosilicate glasses in terms of absorption and scattering losses as well as chemical stability [3], despite having greater refractive indices. Glasses can only be created when tellurium oxide is combined with other compounds, like oxides and halides. Because of its excellent ability to dissolve rare earth elements, tellurium oxide is also

considered as a good dopant. Tellurium oxide has a strong ability to dissolve rare earth ions as dopants and is considered to be a favourable environment for its radiative transitions [4].

The optimal method for creating tellurite glass systems with zinc oxide was based on the traditional melt quenching technique. ZnO, a well-established substance can fully form samples in glassy and amorphous characteristics. Due to ZnO's exceptional properties, it is suggested that better-quality glass can be produced focusing on the targeted parameters which is density, molar volume, ultrasonic velocities, elastic moduli, softening temperature, fractal bond connectivity, micro hardness, Debye temperature, and acoustic impedance [5].

On the other hand, neodymium (III) ion (Nd^{3+}), one of the rare ions doped in glasses, has earned recognition as one of the most efficient. The magnificence of Nd^{3+}'s are anticipated to enable numerous better glass applications, such as frequency up conversion, amplification, and laser emission [6]. Because glasses are so important technologically, a lot of research has been done to explain their structural details. This knowledge helps to clarify the connection between structure and properties, and can be used to develop novel materials, most notably glass with a silicate basis [7].

Graphical representation of the atomic structure of glass is essential for highlighting its amorphous characteristics. There are plenty of methods to visualize this structure such as radial distribution [8], that allows a clear understanding of the nature of glass at the atomic level. These representations are important to distinguish the amorphous structure of materials, known for its key features such as the absence of periodicity and the presence of short-range order. Various tools are already available in the field of material science and more specifically for the analysis and representation of the atomic structure of materials. Examples of these tools include VESTA, Diamond and OVITO [9-10], which offer powerful visualization capabilities for both crystalline and amorphous materials. VESTA and Diamond are particularly user-friendly with graphical interfaces, while OVITO provides advanced visualization and analysis through both GUI and optional Python scripting.

Farrow et al., [11] stands out for its focus on Pair Distribution Function (PDF) analysis, making it ideal for studying the local atomic structure of amorphous materials. One of the tools is RDF Tools which, according to Mitchell & Petersen [12], is a software tool for quantifying short-range ordering in amorphous materials. However, some of these tools often come with certain limitations, such as the need for commercial licenses. Our solution is a Python-based graphical interface designed for the analysis and the representation of glass structures. The interface developed in this article allows users to specify the molecules composing the glass, input the wavelength used in their experiments, and enter the relevant equations directly. Additionally, this article not only uses the Pair Distribution Function (PDF) analysis but also enhances the relevance and accuracy of the atomic structures simulated by using the Monte Carlo simulations. Combining these techniques makes the simulations much more accurate and detailed for the materials studied. Integrating advanced visualization with an intuitive interface is a significant improvement in accessibility and usability, making it an ideal choice for researchers focused on the study of glass structure [12].

In this paper, the ternary glass series of zinc tellurite doped neodymium oxide nanoparticle glasses, including optical properties studies were implemented and navigated to the behaviour of glass. Both the existence of nanoparticles in glass production processes and their physical characteristics were investigated and evaluated. The theoretical predictions and simulations at different neodymium oxide nanoparticle concentrations were used to examine some of the properties of the manufactured glasses like the density and the molar volume of the glass. This study dives into the ML models used and chosen such as Linear Regression and Gradient Boosting Regression.

II. Materials and Method

The main components used in this study are neodymium oxide nanoparticles, Nd2O3 NPs (Assay, Alfa Aesar, 99.9%), zinc oxide, ZnO (Alfar Aeser, 99.9%), and tellurium oxide, TeO2 (Puratronic, Alfa Aesar, 99.9%). The melt-quenching procedure was used to melt the chemical at high temperatures in an atmosphere [34]. In this research, a series of glasses with the chemical composition [(TeO2)0.70(ZnO)0.30] (1-x) (Nd2O3 NPs) x, with x = 0.01 to 0.05 molar fractions, were produced using the melt-quenching method.

To guarantee homogeneity, the weighted chemical mixture was stirred for about 30 minutes using a cylindrical glass rod. The chemical mixture in the alumina crucible was then warmed in an electric furnace for 30 minutes at 400°C. This procedure serves to remove any moisture that may be present in the chemical mixture. The dry mixture was put in a separate furnace that was set to 800°C [13]. The molten mould was transferred to the first electric furnace after the mixture had completely melted [14] and heated for approximately 60 minutes at 400°C to complete the annealing process. Thermal stress was minimised by enabling the glass molecules to cool and organise themselves into a solid state during this process. The final samples were taken out of the furnace and allowed to cool overnight at room temperature.

A. Pair Distribution Function (PDF)

The atomic pair distribution function [PDF, G(r)] is a simple 1D function that contains information about structural correlations in a material. This function describes the distribution of distances between pairs of particles contained within a given volume.

According to Billinge (2008) [15], the atomic PDF, $G(r)$, is defined as:

$$\mathrm{G(r)} = 4.\pi.\mathrm{r}.(\rho(\mathrm{r}) - \rho_0), \quad (1)$$

where $\rho(r)$ is the atomic pair-density, ρ_0 is the average atomic number density and r is the radial distance.

The PDF yields the probability of finding pairs of atoms separated by a distance r. It is obtained by a sine Fourier transformation of the reciprocal space total scattering structure function $S(Q)$ [16]:

$$\mathrm{G(r)} = \frac{2}{\pi}.\int_0^{\infty} \mathrm{Q}.[\mathrm{S(Q)} - 1].\sin(\mathrm{Qr}).\mathrm{dQ} \quad (2)$$

where $S(Q)$ is the corrected, normalized, diffracted intensity I from the sample and Q is the magnitude of the scattering vector [17],

$$\mathrm{Q} = \frac{4.\pi.\sin\theta}{\lambda} \quad (3)$$

One limitation to the PDF analysis is that it may assume all object locations are mutually independent, which is inaccurate for hard objects because it doesn't account for the minimum separation required between them. This can lead to errors in structural parameters derived from PDF analysis. In this study, the intensity I is equal to the count of rays diffracted by the glass in the experiment.

B. Monte Carlo Simulation

The Monte Carlo is a class of computational algorithms that rely on repeated random sampling to obtain numerical results. One of the key principles of this method is Random Sampling, which means that we use the randomness to explore the solution space of a problem. For example, generating random numbers and using them to simulate processes or solve problems. It is important to note that the results form random sampling is then statistically analysed and used to draw conclusions regarding our data [18].

The Monte Carlo method can be used in various fields and to various data. It applies to problems with no probabilistic content as well as to those with inherent probabilistic structure [19]. Here, the Monte Carlo simulation was used to represent the atomic structure of the glass studied. The positions of the atoms were initialised randomly in the material [20].

$$r_i = (x_i, y_i, z_i) \qquad for\ i = 1,2,3,\dots,N$$

The energy of the system is then calculated based on the difference between the interpolated Pair Distribution Function (PDF) value at a given distance and 1. This is a simplified model where deviations from the desired PDF are penalised [21].

$$E = \sum_{i=1}^{N-1} \sum_{j=i+1}^{N} (f(r_i, r_j) - 1)^2 \qquad (4)$$

Here, $f(r_i, r_j)$ is the PDF interpolator value for the distance between atoms $i\ and\ j$. Where A variable as selected randomly and its position was perturbed slightly, while ensuring that the new position is within the simulation box [22]:

$$r_i^{new} = r_i + \Delta r \qquad (5)$$

where Δr is a small random vector.

The new energy of the system (After the perturbation) is calculated and compared with the old one:

$$\Delta E = E_{new} - E_{old} \qquad (6)$$

An acceptance criterion is then applied where the new configuration is accepted if the new energy is lower. On the other hand, a probability based on the Metropolis criterion will be accepted. This Monte Carlo method effectively explores the configuration space, choosing arrangements that match the desired PDF, thereby simulating the atomic structure of the material.

C. Machine Learning Methods for Property Prediction

In this study, different machine learning approaches were employed to predict various physical properties of the TZNnPs glass system (Density and Molar Volume). This study focuses on these two parameters as a starting point, the results can be generalised to predict other parameters in the same data.

A comparison was done between the different approaches, and for each target value (the value that is needed for prediction), the best model was chosen to work with. The problem of this study falls in regression model, where this model relationship is required between a continuous target variable (Density, Molar Volume) and different independent variables.

For the Density of the glass system, the best performing machine learning model was Gradient Boosting Regressor. On the other hand, for the Molar Volume, the model chosen was Linear Regression. These techniques offer valuable tools for uncovering relationships between the experimental Nd nanoparticle data and the target physical properties.

D. Linear Regression

Linear regression is a statistical method for modelling linear relationships between one or more entities (independent variables) and a continuous target variable (dependent variable) [23]. When there is a single feature, it is called a single-variable linear regression and if there are multiple features, it is a multiple linear regression [24]. In the current case, the dependent variable (That can also be called as target value) is the Molar Volume, and the independent variables are the parameters with which is performed based on the experiment: Nd ion concentration (N), molar volume, ultrasonic velocities, elastic moduli, softening temperature, fractal bond connectivity, micro hardness, Debye temperature, and acoustic impedance.

The linear regression model is presented by the following equation [25]:

$$Y = a_0 + a_1.X_1 + a_2.X_2 + \cdots + a_n.X_n \qquad (7)$$

where Y represents the predicted property value, X_i represent the independent variables (Nd nanoparticle data), $a_1, a_2, \dots, a_n$ the slope of the line, and a_0 is the y-intercept.

Linear regression offers several advantages:

1) Interpretability: The coefficients provide insights into the direction and strength of the relationship between the independent and dependent variables [26].

2) Computational Efficiency: Linear regression algorithms are relatively fast to train and can handle large datasets efficiently [27].

3) However, a key limitation of linear regression is its assumption of linearity. If the relationship between the Nd nanoparticle data and the property is non-linear, the model predictions may not be accurate [28].

E. Gradient Boosting Regression

Gradient Boosting is a machine learning technique that combines the predictions from several models to improve the overall predictive accuracy [29]. It is particularly useful for regression and classification problems. In the current case, this is a regression problem, the objective of the study is to predict and model a continuous dependent variable (Density or Molar Volume), using the parameters used in the experiment. The term "gradient" in Gradient Boosting refers to the method of using the gradient of the loss function to minimize errors during training [30]. The "boosting" part of the name implies that the algorithm combines weak predictive models to form a strong learner [31].

In each stage, a regression tree is fit on the negative gradient of the given loss function [32]. The negative gradient represents the direction in which the loss function decreases the most. The new tree is added to the ensemble, adjusting the predictions based on the errors made by the existing trees.

One of the main advantages of Gradient Boosting is its predictive power. It often outperforms other algorithms on a variety of datasets. However, it can be computationally expensive and slow to train, especially with large datasets. It also requires careful tuning of parameters and regularization to avoid overfitting [33]. In the current case, the dataset studied is not large, which won't cause problems in our usage of the Gradient Boosting model.

F. Mathematical formulation

The final prediction of the Gradient Boosting Regressor is an additive combination of individual tree predictions [34]:

$$f(x) = \sum_{m=1}^{M} \gamma_m . h_m(x) \quad (8)$$

where: M is the number of trees (boosting stages), γ_m is the weight (learning rate) for the (m)-th tree, and $h_m(x)$ represents the prediction of the (m)-th tree for input (x).

G. Machine Learning

In machine learning, comparing between the different models tested plays a crucial role in modelling the target value in the best way possible. There are different ways and metrics to compare between the different models tested in the study. The MSE, MAE, RMSE, and R-Squared metrics are the ones mainly used to evaluate the prediction error rates and model performance in regression problems [35]. The metrics used in this study are RMSE and R-Squared.

The RMSE (Root Mean Squared Error) is the error rate by the square root of the difference between the original and predicted values extracted by squared the average difference over the data set [36].

$$RMSE = \sqrt{\frac{1}{N} . \sum_{m=1}^{N} (y_i - \hat{y}_i)^2} \quad (9)$$

where: N is the number of values predicted, $\hat{y}_i$ is the i-th prediction of Y.

Whereas the R-squared (Coefficient of determination) represents the coefficient of how well the values fit compared to the original values. The value from 0 to 1 interpreted as percentages. The higher the value is, the better the model is.

$$R^2 = 1 - \frac{\Sigma (y_i - \hat{y}_i)^2}{\Sigma (y_i - \bar{y})^2} \quad (10)$$

where: $\bar{y}$ is the mean value of the predictions of Y [37].

The objective of the comparison between the different models used will be having an R-Squared very close to 1 and a RMSE closer to 0.

H. Feature Selection for Property Prediction

In this study, all the parameters of the experiment were used to predict the different outcomes that was needed. Nevertheless, there was still a need to select only the relevant features, for the models to become more accurate in the predictions made.

One of the feature selection methods was the use of the Variance Inflation Factor (VIF), which represents how well the variable was explained by other independent variables [38]. As mentioned above, the R^2 value was determined to find out how well an independent variable was described by the other independent variables. A high value of R^2 means that the variable is highly correlated with the other variables. This was captured by the VIF, which was as denoted below [39]:

$$VIF = \frac{1}{1-R^2} \quad (11)$$

Multicollinearity can be a problem in a regression model, because the estimated regression coefficients become unstable and difficult to interpret in the presence of multicollinearity. This is where the VIF interferes since it can show the correlation of a variable with a group of other variables. It captures the multicollinearity of the variables that we use. The closer the R^2 value to 1, the higher the value of VIF and the higher the multicollinearity in the dataset.

III. Results and Discussion

A. Glass Analysis

In order to confirm the structure of glass, Figure 1 depicts the X-ray diffraction (XRD) spectra of TZNnPs. A large hump with no clearly visible sharp peaks can be seen in the glass' XRD pattern at 20 to 35 degrees. These spectra show the traits of an amorphous structure, proving that a crystalline phase is not present [40–41].

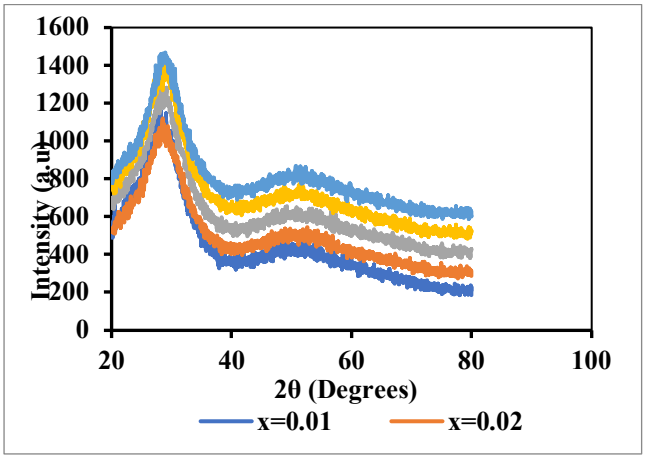

Fig. 1 XRD pattern of the TZNnPs glass system

To validate the experimental results, the Pair Distribution Function (PDF) was plotted alongside the experimentally obtained data. As illustrated in Figure 2, the graph reveals a striking similarity between the experimental data and the PDF, particularly in the curve's form. This strong correlation underscores the reliability of the experimental findings, affirming their accuracy and consistency with theoretical expectations [42].

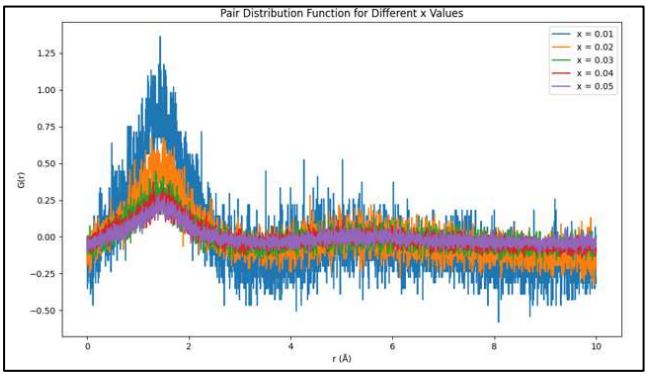

Fig. 2 Pair Distribution Function for TZNnPs glass system

To validate the experimental results and visualise the atomic structure of the studied material, a Python-based graphical user interface (GUI) was adopted. Figure 3 illustrates this interface, which includes features such as input fields for wavelength, components of the material, and the ability to upload an Excel file containing experimental data. This GUI enables users to effectively manage and analyse complex datasets, providing a robust platform for visualising atomic structures and confirming experimental findings. Such tools are essential for advancing materials science research by offering user-friendly environments for detailed data analysis and visualisation [43].

Fig. 3 Python-based GUI developed

After using the Pair Distribution Function (PDF) and Monte Carlo simulations, the atomic structure was examined for varying concentrations. Figure 4 illustrates the results, highlighting that the Monte Carlo simulations, depicted in the second row, outperform the PDF in revealing the amorphous nature of the glass used in the experiments. The effectiveness of Monte Carlo simulations in accurately modelling disordered materials and providing insights into the atomic structure has been well-documented in the literature [44 - 45]. These simulations are particularly advantageous for understanding the complex, non-crystalline structures often found in amorphous materials.

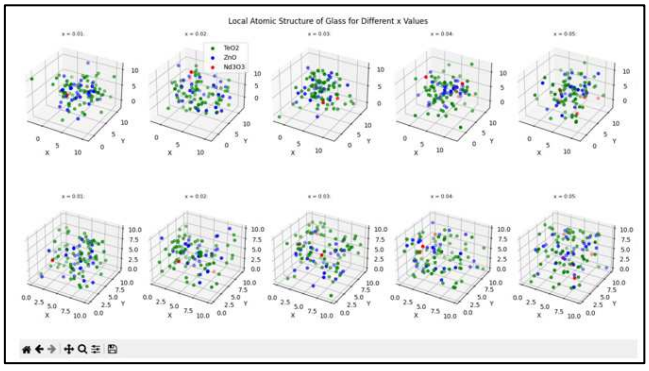

Fig. 4 Atomic structure for TZNnPs glass system and with Monte Carlo and PDF

To visualise the different structures obtained, especially the difference between the usage or not of the Monte Carlo simulation. The graphs of the atomic structure were plotted for a specific density. Figure 5 shows how the Monte Carlo enhances and highlights the amorphous structure of the glass used in the experiments.

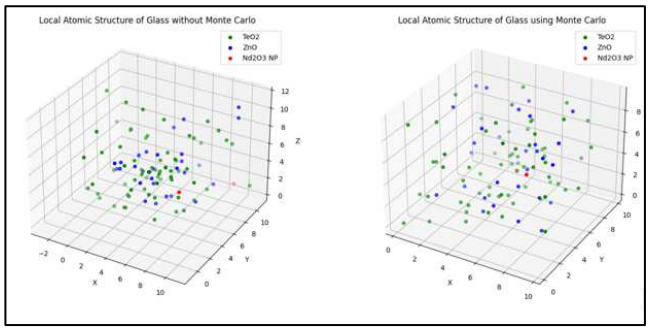

Fig. 5 Comparison between Atomic Structures with Monte Carlo and with PDF only

B. *Machine Learning Approach*

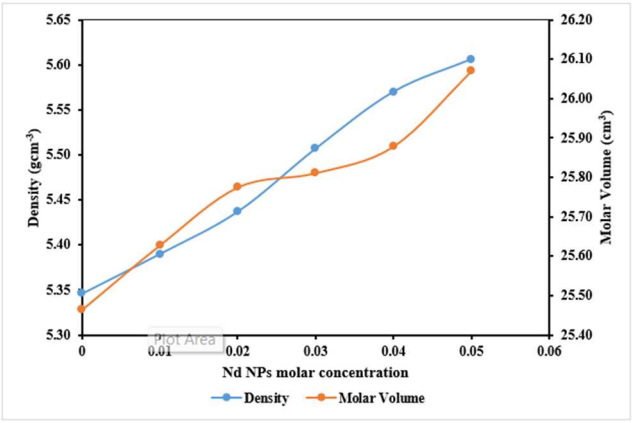

Fig. 6 Density and molar volume variation with Nd NPs molar concentration in TZNnPs glass system

The discrepancy between the TZNnPs glasses' density and molar volume values is shown in Figure 6. As the concentration of Nd_2O_3 NPs climbs from 0.01 to 0.05 molar fraction, the density of the produced glasses increased from 5346 to 5580 kg/m^3. This was because heavier Nd_2O_3 NPs replaced lighter ZnO atoms thus, increased the glass's overall average molecular weight [44].

The molar volume grew from 25.464 cm^3/mol to 26.192 cm^3/mol as the concentration of Nd_2O_3 NPs increased from 0.01 to 0.05 molar fraction. The molar volume increased as Nd_2O_3 NP concentration rised due to the presence of more non-bridging oxygen molecules. (NBO). Glass containing neodymium oxide serves as a modifier by occupying network interstices and introducing additional neodymium boron oxide (NBO) into the structure. The presence of Nd2O3 NPs may ultimately caused the glass network to stretch [46]. Since x is bigger than 0.02 molar fraction, the increase in molar volume might be caused by the smaller Te and Zn atoms being replaced by larger Nd atoms. The present study shows that as Nd_2O_3 NP concentration rises, the glasses' molar volume rises as well. Therefore, an increase in molar volume is equivalent to an increase in the open volume of the glass network [46].

In order to have an idea about the glass' behaviour towards Nd_2O_3 NPs concentration change prior to future experiments, the data was used from this experiment to develop a Machine Learning tool to predict the values of density and molar volume based on the other physical properties of the glass [47].

This section presents the results of the machine learning predictions for the following target properties: density, and

molar volume [48]. The dataset comprised both experimental data points and synthesised data points for Nd_2O_3 nanoparticles (NPs), representing the molar fraction of Nd_2O_3 in the glass system. To enhance the robustness and generalisation capability of the predictive models, the experiment was repeated numerous times with different scenarios.

B. Density Prediction

The analysing of the data began as well as defining the best model to use for each prediction based on metrics like RMSE and R^2 score [49]. Below are the best five models for the prediction of density given by the comparison models' function obtained from pycaret.regression library [50]:

TABLE I
RANKING OF THE 5 BEST MODELS FOR THE DENSITY'S PREDICTION (USING COMPARE MODELS)

	Model	RMSE	R2
gbr	Gradient Boosting Regressor	0.0055	0.9938
et	Extra Trees Regressor	0.0057	0.9935
ada	AdaBoost Regressor	0.0065	0.9906
dt	Decision Tree Regressor	0.0065	0.9901
xgboost	Extreme Gradient Boosting	0.0088	0.9841

The prediction of density was proceeded using these models. The dataset started to randomise and dividing it into a training set (67%) and a testing set (33%) [51]. The models were trained using the training set and were then used to predict the values of density, whilst their performance was evaluated using the RMSE and R^2 score [49]. The curves of the values predicted by the models were plotted and compared to the actual experimental values of density. The result is as follows:

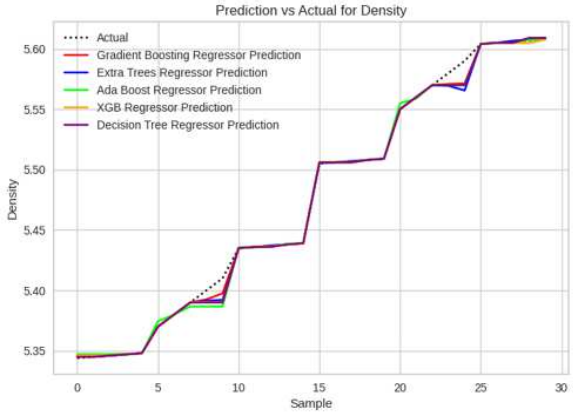

Fig. 7 Graph of predicted values of density using the different models compared to actual values

The RMSE and R^2 scores of the different models are presented in the Table 2:

TABLE II
RMSE AND R^2 METRICS FOR THE BEST 5 MODELS FOR THE DENSITY 'S PREDICTION

Model	Gradient Boosting	Extra Trees	Ada Boost	XGB	Decision Tree
RMSE	0.00464	0.00608	0.00659	0.00571	0.00580
R^2score	0.99756	0.99581	0.99508	0.99630	0.99619

Based on these results, it can be concluded that the best performing model is the Gradient Boosting Regressor. Thus, this model will be elucidated and applied in the prediction of density. In order to improve the model's RMSE and R^2 score, the feature selection need to be executed by measuring each feature's importance and the correlation between the features [52].

TABLE III
FEATURE IMPORTANCE TABLE FOR THE DENSITY'S PREDICTION

Feature	Importance
F	0.342446
N	0.311603
$\triangle E$	0.180110
Concentration	0.026311
R_m	0.021963
OPD	0.020850
χ	0.019286
$E^{1/2}$	0.018584
M	0.017427
ε_{opt}	0.008868
Vm	0.006662
α_m	0.006043
E^2	0.004871
α_{me}	0.004685
Λ_{th}	0.004203
ε	0.002209
R_p	0.001264
α_e	0.001202
R_i	0.000884
n	0.000528

Using this important comparison, the least important features was removed and the impact on the RMSE and R^2 score was observed. When the least important feature "n" was removed, a RMSE was obtained amounting of 0.003595 and R^2 score of 0.99854 thus, the accuracy of the prediction improves. Whereas, when two features: "n" and "R_i" were removed, we got RMSE = 0.0049998 and R^2 = 0.99717, which decreased the quality of the prediction. It can be concluded that the importance of the parameters of the features calculated is not enough to do the feature selection and improve the accuracy of the model since there can be underlying multicollinearities between the features. What is of importance, is that an indicator calculated by a function in

the code that measures is based on the dataset, and what features the model used, are more important in the prediction. To identify these multicollinearities [53], the correlation matrix was depicted, as well as performing a y-data profiling using the pandas-profiling library to generate a comprehensive data profiling report. The ProfileReport class from this library provided a quick and easy way to create a detailed report that included aspects on statistics, correlations, and visualisations for both the target variable and the entire dataset. [53].

The correlation matrix looks as follows:

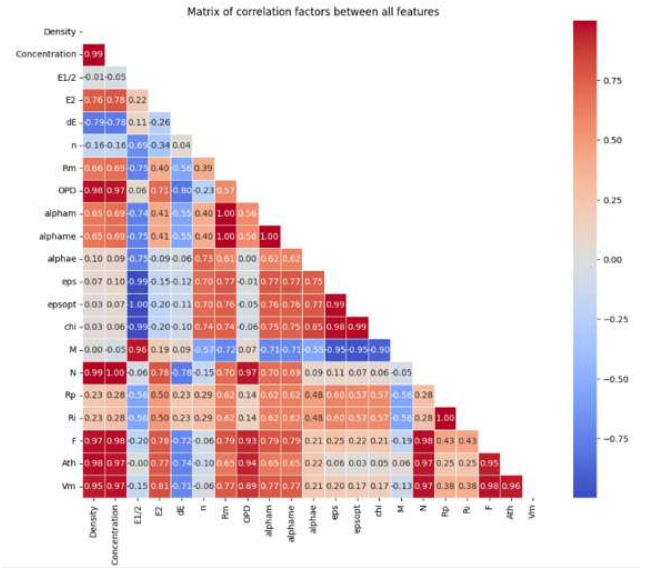

Fig. 8 Matrix of correlation factors between all features

The y-data profiling provides a report including alerts presented below:

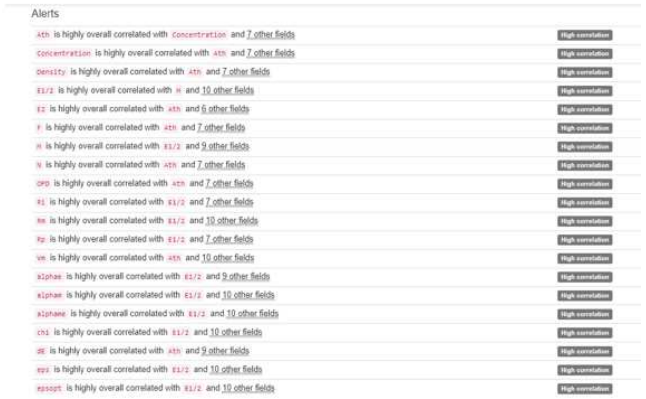

Fig. 9 Overview of the Profile Report's alerts using ydata profiling

To decide which of these highly correlated features to be removed to improve the model's predictions, the Variance Inflation Factor (VIF) was calculated for each feature. This helped to prevent multicollinearity. This is a situation where two or more features in a regression model are highly correlated with each other [54]. Multicollinearity can distort the results of the model and make it difficult to determine the individual effect of each feature on the target variable. The values of the VIFs calculated are presented in the table below:

TABLE IV
VIF VALUES FOR THE DIFFERENT FEATURES USED IN THE PREDICTION OF THE DENSITY

Feature	VIF	Feature	VIF
Concentration	∞	ε	1.251825e+02
$E^{1/2}$	∞	ε_{opt}	∞
E^2	∞	χ	∞
△E	∞	M	∞
n	8.803430e+00	N	∞
R_m	∞	R_p	∞
OPD	4.503600e+15	R_i	1.055298e+06
α_m	∞	F	∞
α_{me}	∞	Λ_{th}	∞
α_e	∞	Vm	∞

Based on the VIF values, it was decided to remove the features with infinite VIF values [56]. After doing this, the following prediction was obtained:

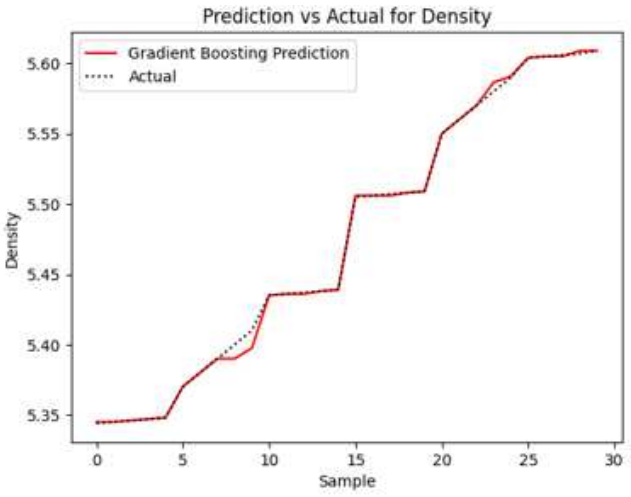

Fig. 10 Graph of predicted values of density after removing the highly correlated features compared to actual values

The RMSE of this new prediction was 0.0032 and R^2 = 0.9988, which were the best scores obtained from all the predictions performed previously. It can be concluded that for an accurate prediction of density, the use of Gradient Boosting Regressor as a model was required, and the features "n", "OPD", "ε" and "R_i" as the prediction variables.

To comprehend the optical characteristics of glass, two essential quantities are the refractive index, 'n', and the optical packing density (OPD). By measuring the degree of refraction as light enters glass from another medium, the refractive index establishes how light travels through the material [55]. This characteristic, which affects the focusing power and clarity of the glass, is crucial for building lenses and other optical components. For applications like eyeglasses and cameras, slimmer lenses with the same optical power are possible with a higher refractive index. The refractive index is also influenced by optical packing density, which is the measure of how closely atoms or molecules are packed within the

glass. Higher refractive indices and superior mechanical qualities of denser materials make them appropriate for high-performance optical applications [56].

Glass's optical characteristics are further influenced by the dielectric constant and internuclear distance. The material's capacity to store electrical energy in an electric field, which influences wave propagation, polarisation, and light interaction, is measured by the dielectric constant. When it comes to optical equipment like modulators and capacitors, a larger dielectric constant can improve function [57]. This characteristic also sheds light on the constancy and purity of the material, which are essential for dependable and effective optical systems. The average distance between the atoms' nuclei within a glass, or the inter-nuclear distance, influences the atomic structure and bonding properties of the material. Stronger bonding is typically indicated by shorter distances, which improve the mechanical strength and thermal stability of the glass. This parameter also affects the electrical and vibrational characteristics of the glass, affecting its emission and absorption spectra, which is important for laser applications [58].

IV. *Molar Volume Prediction*

For the Molar Volume prediction, the same way was proceeded as for density, starting by defining the best 5 models to use, with the following RMSE and R^2:

TABLE V
RANKING OF THE 5 BEST MODELS FOR THE MOLAR VOLUME'S PREDICTION (USING COMPARE MODELS)

	Model	RMSE	R2
lr	Linear Regression	0.0042	0.9987
br	Bayesian Ridge	0.0075	0.9974
et	Extra Trees Regressor	0.0112	0.9878
gbr	Gradient Boosting Regressor	0.0127	0.9782
huber	Huber Regressor	0.0142	0.9655

Then, the same splitting ratios were used for the training and testing sets. The prediction plots compared to the experimental values are presented below:

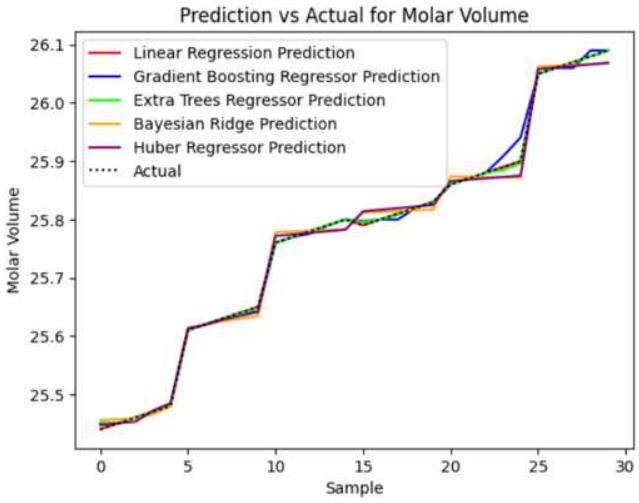

Fig. 11 Graph of predicted values of density after removing the highly correlated features compared to actual values

The RMSE and R^2 for these predictions are as follows:

TABLE VI
RSME AND R^2 METRICS FOR THE BEST 5 MODELS FOR THE MOLAR VOLUME'S PREDICTION

Model	RMSE	R^2 score
Linear Regression	2.67439 e-15	1.0000
Bayesian Ridge	0.012351	0.995852
Extra Trees	0.002733	0.999797
Gradient Boosting	0.009199	0.997699
Huber Regressor	0.010933	0.996750

As depicted in Table 6, the linear regression provides the best R^2 and RMSE values for the prediction of the Molar Volume. Thus, it can be concluded that it's the best model to be used. It is also important to note that no further feature selection is needed to improve the model, unlike the prediction of the density done previously with the Gradient Boosting, where the model used needed improvements via feature selection [54].

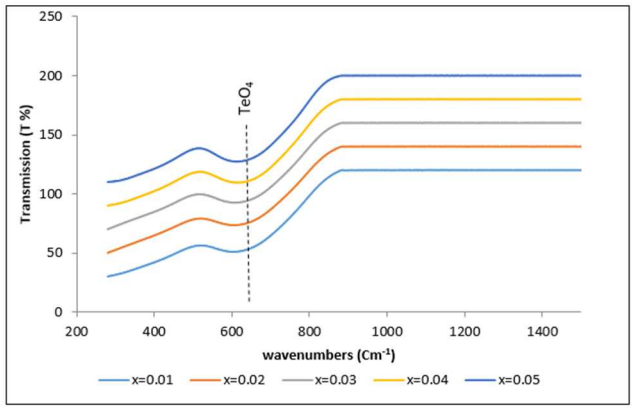

Fig. 12 FTIR Spectra for the TZNnPs glass system

Further study was conducted using Fourier transform infrared (FTIR) spectroscopy based on the crystallinity of the glass matrices. The details of the chemical bond between the elements were revealed by the FTIR findings [59]. Two crucial structural features differentiate the tellurite oxide structure, a trigonal bipyramid (TeO_4) and trigonal pyramid. (TeO_3). Pure TeO_2's absorption band was visible at 640 cm^{-1}, and the trigonal bipyramid (TeO_4) and trigonal pyramid's stretching wave were both visible between 600 and 700 cm^{-1}. (TeO_3). Between 650 and 700 cm^{-1}, TeO_3 had a stretching band, while TeO_4 had an oscillation band between 600 and 650 cm^{-1} [60]. Figure 12 displays the FTIR spectra that were obtained between 250 and 1300 cm-1 and comprised the kind of bonding that was taking place. Between 600 and 700 cm^{-1}, the two structural elements of the tellurium oxide pattern were visible. The major band, which was linked to the symmetrical pyramid of the TeO_4 structural unit, was discernible between 603.23 and 632.74 cm^{-1} [61].

Since the ZnO band was presented but offered no spectral information, the zinc lattice had entirely disintegrated. TeO_4 samples were produced. This strongly binds oxygen anions to the glass network. Consequently, as the TeO_4 concentration rises, the amount of non-bridging oxygen decreases and vice versa [62]. Additionally, the transmission spectra were converted into absorption spectra in order to ascertain the TeO_4 content. The TeO_4 content in the glass was then

represented by the area under the TeO_4 absorption curve. Origin 6.0 software was used to look at the area under the absorption graph and calculate the concentration. Table 7 and Figure 13 show the different TeO_4 concentrations in comparison to the Nd molar fraction.

TABLE VII
BAND CENTER (B), BAND AREA (A), (TEO4, TEO3) CONCENTRATION FOR TZNNPS GLASS SYSTEM

Nd_2O_3 mol content		TeO_4 trigonal bipyramid	TeO_3 trigonal pyramid	TeO_4 Concentration	TeO_3 Concentration
0.00	B	607.481	680.372	0.235	0.765
	A	21.221	69.243		
0.01	B	603.234	678.681	0.298	0.702
	A	29.585	69.582		
0.02	B	618.791	654.650	0.115	0.885
	A	6.805	52.338		
0.03	B	632.740	677.792	0.107	0.893
	A	7.650	63.741		
0.04	B	614.011	676.841	0.235	0.765
	A	21.253	68.998		
0.05	B	611.770	662.202	0.510	0.4905
	A	28.435	27.372		

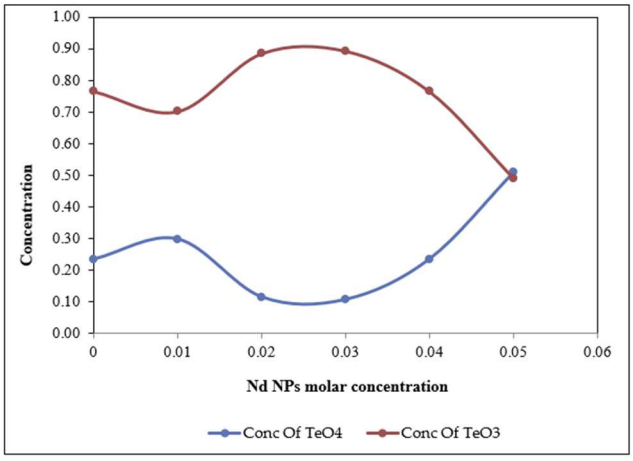

Fig. 13 TeO4 and TeO3 contraction variation with Nd NPs molar concentration in TZNnPs glass system

In this experiment, an increasing amount of non-bridging oxygen was rectified by a decreasing amount of TeO_4 as the quantity of Nd^{3+} ions increased from 0.01 to 0.02 molar content. Additionally, as the Nd^{3+} ion concentration rose from 0.02 to 0.05 molar concentration of Nd_2O_3 NPs, the TeO_4 concentration then rose gradually. The additional bridging oxygen (BOs) had resulted in a more densely packed network, which was reflected by the rise in TeO_4 content [63]. The glass network's arrangement of trigonal pyramidal TeO_3 structural units supported the development of a bridge oxygen and the change from TeO_3 to TeO_4 [64].

Additionally, Figure 14 displays TEM images of TZNnPs glass with a 0.03 molar percentage. The TEM images showed the microstructure of the glasses, which held nanoparticles of various sizes (74 nm). Neodymium nanoparticles were found to aggregate once they were incorporated into the glass matrix, which is similar to their typical size as unprocessed particles, which ranges from 15 to 30 nm. The bigger particle size after glass formation is brought on by the Ostwald ripening, in which smaller particles diffuse to larger particles [65]. In addition, the nanoparticles could also enhance the absorption and emission properties. From the phenomenon, a few potential mechanisms promoting application can develop such as quantum dots and photonic effect.

In quantum dots, semiconductor nanoparticles are embedded in glass. This scenario can introduce size-tunable absorption and emission properties, which are useful in applications such as lasers, displays, and bio-imaging. However, under photonic effect, nanoparticles can create photonic bandgap structures within the glass, affecting how light propagates through the material and enabling applications in photonic crystals and waveguides.

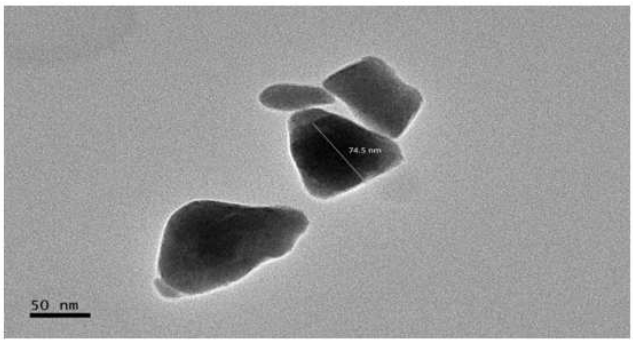

Fig. 13 The TEM morphology of TZNnPs, x = 0.03 molar content glass

IV. CONCLUSION

The glasses TZNnPs under study revealed that the molar volume and density rose from 25,7066 to 26,3452 cm3 and 5346 to 5606 kg m^{-3}, respectively. Studies of the crystallinity, structural changes, and morphological structures of the glasses were conducted using XRD, FTIR, and TEM observations. Studies using the Python-Based GUI showed that the atomic structure is amorphous. When we increase the concentration of Nd_2O_3 NP, the amorphous characteristics of the glass are more apparent. This interface can also serve other studies, using new molecules and materials. Furthermore, ML models used to predict the different properties showed great performance as shown not only by the graphs comparing the predictions to the actual values but also with the metrics used to evaluate their performances such as the R-Squared and the RMSE.

The best model for the prediction of the density was Gradient Boosting Regressor. It is important to note that a feature selection and visualisation was done afterwards, showing that there are some parameters that contribute more than others to the prediction process. This is due to the multicollinearity present between some of the features. Whereas for the prediction of the molar volume, the best performing model was Linear Regression. To conclude, this study could be generalised to the predictions of the other parameters of the glass, and with more data, the models chosen will be able to perform even better.

ACKNOWLEDGMENT

This work was supported by Tenaga Nasional Berhad (TNB) and UNITEN through Tan Sri Leo Moggie

Distinguished Chair in Energy Informatics, Institute of Informatics and Computing in Energy (IICE), UNITEN under the code 2021EIChair

REFERENCES

[1] M. J. C. Mauro, "Topological constraint theory of glass," *American Ceramic Society Bulletin*, vol. 90, no. 4, pp. 31, 2011.

[2] I. S. Mustafa, N. A. N. Razali, A. R. Ibrahim, N. Z. Yahaya, and H. M. Kamari, "From rice husk to transparent radiation protection material," *Jurnal Intelek*, vol. 9, no. 2, 2015.

[3] P. Damas, J. Coelho, G. Hungerford, and N. S. Hussain, "Structural studies of lithium boro tellurite glasses doped with praseodymium and samarium oxides," *Materials Research Bulletin*, vol. 47, no. 11, pp. 3489–3494, Nov. 2012, doi: 10.1016/j.materresbull.2012.06.071.

[4] M. S. Gaafar, M. A. M. Abdeen, and S. Y. Marzouk, "Structural investigation and simulation of acoustic properties of some tellurite glasses using artificial intelligence technique," *Journal of Alloys and Compounds*, vol. 509, no. 8, pp. 3566–3575, Feb. 2011, doi: 10.1016/j.jallcom.2010.12.064.

[5] S. H. Alazoumi, H. A. A. Sidek, M. K. Halimah, K. A. Matori, M. H. M. Zaid, and A. A. Abdulbaset, "Synthesis and Elastic Properties of Ternary ZnO-PbO-TeO_2 Glasses," *Chalcogenide Letters*, vol. 14, no. 8, 2017.

[6] C. Bootjomchai, "Comparative studies between theoretical and experimental of elastic properties and irradiation effects of soda lime glasses doped with neodymium oxide," *Radiation Physics and Chemistry*, vol. 110, pp. 96–104, May 2015, doi:10.1016/j.radphyschem.2015.01.034.

[7] W. Chinnamat, R. Laopaiboon, J. Laopaiboon, S. Pencharee, and C. Bootjomchai, "Influence of ionic radius modifying oxides on the elastic properties of glasses using ultrasonic techniques and FTIR spectroscopy," *Physics and Chemistry of Glasses: European Journal of Glass Science and Technology Part B*, vol. 58, no. 5, pp. 207–216, Oct. 2017, doi: 10.13036/17533562.58.5.101.

[8] D. Srolovitz, T. Egami, and V. Vitek, "Radial distribution function and structural relaxation in amorphous solids," *Physical Review B*, vol. 24, no. 12, pp. 6936–6944, Dec. 1981, doi: 10.1103/physrevb.24.6936.

[9] P. Siroha, D. Singh, R. Soni, and J. Gangwar, "Comparative study on crystallographic representation of transition metal oxides polymorphs nanomaterials using VESTA software: Case study on Fe2O3 and TiO2," *AIP Conference Proceedings*, vol. 2006, p. 030038, 2018, doi:10.1063/1.5051294.

[10] S. Abdullah, X. Zhou, R. Aguirre, and D. Zubia, "A computational approach to analyze grain structures of semiconductor compound films: Case study of CdTe/CdS multilayers," *MRS Advances*, vol. 7, no. 22, pp. 457–461, Jan. 2022, doi: 10.1557/s43580-021-00194-y.

[11] C. L. Farrow et al., "PDFfit2 and PDFgui: computer programs for studying nanostructure in crystals," *Journal of Physics: Condensed Matter*, vol. 19, no. 33, p. 335219, Jul. 2007, doi: 10.1088/0953-8984/19/33/335219.

[12] D. R. G. Mitchell and T. C. Petersen, "RDFTools: A software tool for quantifying short-range ordering in amorphous materials," *Microscopy Research and Technique*, vol. 75, no. 2, pp. 153–163, Jul. 2011, doi: 10.1002/jemt.21038.

[13] V. Dimitrov and T. Komatsu, "An interpretation of optical properties of oxides and oxide glasses in terms of the electronic ion polarizability and average single bond strength," *J. Univ. Chem. Technol. Metall.*, vol. 45, no. 3, pp. 219–250, 2010.

[14] D. Linda et al., "Optical properties of tellurite glasses elaborated within the TeO2–Tl2O–Ag2O and TeO2–ZnO–Ag2O ternary systems," *Journal of Alloys and Compounds*, vol. 561, pp. 151–160, Jun. 2013, doi: 10.1016/j.jallcom.2013.01.172.

[15] S. J. L. Billinge, "Nanoscale structural order from the atomic pair distribution function (PDF): There's plenty of room in the middle," *Journal of Solid State Chemistry*, vol. 181, no. 7, pp. 1695–1700, Jul. 2008, doi: 10.1016/j.jssc.2008.06.046.

[16] R. Sharma and A. Tenguria, "Some new techniques in the approximation of q-special function," 2019.

[17] T. T. Larsen-Olsen et al., "Simultaneous multilayer formation of the polymer solar cell stack using roll-to-roll double slot-die coating from water," *Solar Energy Materials and Solar Cells*, vol. 97, pp. 22–27, Feb. 2012, doi: 10.1016/j.solmat.2011.08.026.

[18] R. Y. Rubinstein and D. P. Kroese, *Simulation and the Monte Carlo Method*, 2nd ed. Hoboken, NJ, USA: John Wiley & Sons, 2016.

[19] G. Fishman, *Monte Carlo: Concepts, Algorithms, and Applications*, New York, USA: Springer, 1996.

[20] N. P. Kisbye, "The integral kernel in the kuznetsov type sum formula for SU(n + 1, 1)," *Indagationes Mathematicae*, vol. 12, no. 1, pp. 83–101, 2001, doi: 10.1016/s0019-3577(01)80007-0.

[21] W. Wang, "Existence of closed characteristics on compact convex hypersurfaces in $$\mathbf{R}^{2n}$$ R 2 n," *Calculus of Variations and Partial Differential Equations*, vol. 55, no. 1, Jan. 2016, doi:10.1007/s00526-015-0945-8.

[22] V. Springel, R. Pakmor, O. Zier, and M. Reinecke, "Simulating cosmic structure formation with the gadge-4 code," *Monthly Notices of the Royal Astronomical Society*, vol. 506, no. 2, pp. 2871–2949, Jul. 2021, doi: 10.1093/mnras/stab1855.

[23] T. R. Vetter and P. Schober, "Regression: The Apple Does Not Fall Far From the Tree," Anesthesia & Analgesia, vol. 127, no. 1, pp. 277–283, Jul. 2018, doi: 10.1213/ane.0000000000003424.

[24] M. Tranmer and M. Elliot, "Multiple linear regression," *The Cathie Marsh Centre for Census and Survey Research (CCSR)*, vol. 5, no. 5, pp. 1–5, 2008.

[25] L. J. Yang, M. J. Bibby, and R. S. Chandel, "Linear regression equations for modeling the submerged-arc welding process," *Journal of Materials Processing Technology*, vol. 39, no. 1–2, pp. 33–42, Oct. 1993, doi: 10.1016/0924-0136(93)90006-r.

[26] M. Z. Naser, "An engineer's guide to eXplainable Artificial Intelligence and Interpretable Machine Learning: Navigating causality, forced goodness, and the false perception of inference," *Automation in Construction*, vol. 129, p. 103821, Sep. 2021, doi:10.1016/j.autcon.2021.103821.

[27] J. Wu and H. Yang, "Linear Regression-Based Efficient SVM Learning for Large-Scale Classification," *IEEE Transactions on Neural Networks and Learning Systems*, vol. 26, no. 10, pp. 2357–2369, Oct. 2015, doi: 10.1109/tnnls.2014.2382123.

[28] A. S. Barnard, "Challenges in modelling nanoparticles for drug delivery," *Journal of Physics: Condensed Matter*, vol. 28, no. 2, p. 023002, Dec. 2015, doi: 10.1088/0953-8984/28/2/023002.

[29] Y. Zhang and A. Haghani, "A gradient boosting method to improve travel time prediction," *Transportation Research Part C: Emerging Technologies*, vol. 58, pp. 308–324, Sep. 2015, doi:10.1016/j.trc.2015.02.019.

[30] A. Natekin and A. Knoll, "Gradient boosting machines, a tutorial," *Frontiers in Neurorobotics*, vol. 7, 2013, doi:10.3389/fnbot.2013.00021.

[31] A. J. Ferreira and M. A. T. Figueiredo, "Boosting Algorithms: A Review of Methods, Theory, and Applications," *Ensemble Machine Learning*, pp. 35–85, 2012, doi: 10.1007/978-1-4419-9326-7_2.

[32] L. Guelman, "Gradient boosting trees for auto insurance loss cost modeling and prediction," *Expert Systems with Applications*, vol. 39, no. 3, pp. 3659–3667, Feb. 2012, doi: 10.1016/j.eswa.2011.09.058.

[33] R. Moradi, R. Berangi, and B. Minaei, "A survey of regularization strategies for deep models," *Artificial Intelligence Review*, vol. 53, no. 6, pp. 3947–3986, Dec. 2019, doi: 10.1007/s10462-019-09784-7.

[34] P. Nie, M. Roccotelli, M. P. Fanti, Z. Ming, and Z. Li, "Prediction of home energy consumption based on gradient boosting regression tree," *Energy Reports*, vol. 7, pp. 1246–1255, Nov. 2021, doi:10.1016/j.egyr.2021.02.006.

[35] D. Chicco, M. J. Warrens, and G. Jurman, "The coefficient of determination R-squared is more informative than SMAPE, MAE, MAPE, MSE and RMSE in regression analysis evaluation," *PeerJ Computer Science*, vol. 7, p. e623, Jul. 2021, doi: 10.7717/peerj-cs.623.

[36] A. Morteza, M. Sadipour, R. S. Fard, S. Taheri, and A. Ahmadi, "A dagging-based deep learning framework for transmission line flexibility assessment," *IET Renewable Power Generation*, vol. 17, no. 5, pp. 1092–1105, Dec. 2022, doi: 10.1049/rpg2.12663.

[37] S. N. Chakrabartty, "Improving linearity in health science investigations," *Health Science Journal*, vol. 17, no. 4, pp. 1–6, 2023.

[38] J. Cheng, J. Sun, K. Yao, M. Xu, and Y. Cao, "A variable selection method based on mutual information and variance inflation factor," *Spectrochimica Acta Part A: Molecular and Biomolecular Spectroscopy*, vol. 268, p. 120652, Mar. 2022, doi:10.1016/j.saa.2021.120652.

[39] R. Salmerón Gómez, A. Rodríguez Sánchez, C. G. García, and J. García Pérez, "The VIF and MSE in Raise Regression," *Mathematics*, vol. 8, no. 4, p. 605, Apr. 2020, doi: 10.3390/math8040605.

[40] Q. Li et al., "Er 3+ /Yb 3+ co-doped bioactive glasses with up-conversion luminescence prepared by containerless processing,"

Ceramics International, vol. 42, no. 11, pp. 13168–13175, Aug. 2016, doi: 10.1016/j.ceramint.2016.05.108.

[41] A. A. A. Awshah et al., "Effect of Neodymium Nanoparticles on Elastic Properties of Zinc-Tellurite Glass System," *Advances in Materials Science and Engineering*, vol. 2017, pp. 1–7, 2017, doi:10.1155/2017/6790635.

[42] A. S. Masadeh, "Total scattering atomic pair distribution function: new methodology for nanostructure determination," *Journal of Experimental Nanoscience*, vol. 11, no. 12, pp. 951–974, May 2016, doi: 10.1080/17458080.2016.1184769.

[43] A. Stukowski, "Visualization and Analysis Strategies for Atomistic Simulations," *Multiscale Materials Modeling for Nanomechanics*, pp. 317–336, 2016, doi: 10.1007/978-3-319-33480-6_10.

[44] M. Fábián et al., "Network structure and thermal properties of bioactive (SiO2–CaO–Na2O–P2O5) glasses," *Journal of Materials Science*, vol. 55, no. 6, pp. 2303–2320, Nov. 2019, doi:10.1007/s10853-019-04206-z.

[45] K. Németh et al., "Efficient simultaneous reverse Monte Carlo modeling of pair-distribution functions and extended x-ray-absorption fine structure spectra of crystalline disordered materials," *The Journal of Chemical Physics*, vol. 136, no. 7, Feb. 2012, doi:10.1063/1.3684547.

[46] S. B. Adamu et al., "Structural, prediction and simulation of elastic properties for tellurite based glass systems doped with nano and micro Eu2O3 particles via artificial neural network model," *Journal of Materials Research and Technology*, vol. 17, pp. 586–600, Mar. 2022, doi: 10.1016/j.jmrt.2022.01.035.

[47] G. E. Karniadakis, I. G. Kevrekidis, L. Lu, P. Perdikaris, S. Wang, and L. Yang, "Physics-informed machine learning," *Nature Reviews Physics*, vol. 3, no. 6, pp. 422–440, 2021.

[48] J. Singh and S. Singh, "A review on Machine learning aspect in physics and mechanics of glasses," *Materials Science and Engineering: B*, vol. 284, p. 115858, Oct. 2022, doi:10.1016/j.mseb.2022.115858.

[49] V. Tatachar, "Comparative assessment of regression models based on model evaluation metrics," *International Journal of Innovative Technology and Exploring Engineering*, vol. 8, no. 9, pp. 853–860, 2021.

[50] E. A. Mohammed, M. A. Naaj, M. Nachouki, and R. Mehdi, "Predicting Student Grade Point Average: Comparison of Machine Learning Regression Algorithms," *2023 24th International Arab Conference on Information Technology (ACIT)*, vol. 18, pp. 1–6, Dec. 2023, doi: 10.1109/acit58888.2023.10453712.

[51] M. K. Uçar, M. Nour, H. Sindi, and K. Polat, "The Effect of Training and Testing Process on Machine Learning in Biomedical Datasets," *Mathematical Problems in Engineering*, vol. 2020, pp. 1–17, May 2020, doi: 10.1155/2020/2836236.

[52] B. Venkatesh and J. Anuradha, "A Review of Feature Selection and Its Methods," *Cybernetics and Information Technologies*, vol. 19, no. 1, pp. 3–26, Mar. 2019, doi: 10.2478/cait-2019-0001.

[53] J. Y.-L. Chan et al., "Mitigating the Multicollinearity Problem and Its Machine Learning Approach: A Review," *Mathematics*, vol. 10, no. 8, p. 1283, Apr. 2022, doi: 10.3390/math10081283.

[54] G. James, D. Witten, T. Hastie, and R. Tibshirani, *An introduction to statistical learning*, vol. 112, p. 18, New York: Springer, 2013.

[55] N. M. Nor et al., "Physical, structural and optical characterization of silica-borotellurite glasses containing vanadium and nickel ions," *Physica B: Condensed Matter*, vol. 627, p. 413553, Feb. 2022, doi:10.1016/j.physb.2021.413553.

[56] J. S. Alzahrani, I. H. Midala, H. M. Kamari, N. M. Al-Hada, C. K. Tim, N. N. S. Nidzam, and M. S. Al-Buriahi, "Effect of calcination temperature on the structural and optical properties of $(ZnO)_{0.8}(ZrO_2)_{0.2}$ nanoparticles," *Journal of Inorganic and Organometallic Polymers and Materials*, vol. 32, no. 5, pp. 1755–1765, 2022.

[57] S. N. Nazrin et al., "Thermal and radiation shielding characteristics of erbium ions doped zinc tellurite glasses," *Progress in Nuclear Energy*, vol. 168, p. 104995, Mar. 2024, doi: 10.1016/j.pnucene.2023.104995.

[58] N. Almousa et al., "Tailoring perovskite ceramics for improved structure, vibrational behaviors and radiation protection: The role of lanthanum in PbTiO3," *Optical Materials*, vol. 152, p. 115543, Jun. 2024, doi: 10.1016/j.optmat.2024.115543.

[59] M. N. Azlan, M. K. Halimah, S. O. Baki, and W. M. Daud, "Effect of Neodymium Concentration on Structural and Optical Properties of Tellurite Based Glass System," *Materials Science Forum*, vol. 846, pp. 183–188, Mar. 2016, doi: 10.4028/www.scientific.net/msf.846.183.

[60] S. S. Hajer, M. K. Halimah, Z. Azmi, and M. N. Azlan, "Optical properties of zinc-borotellurite doped samarium," *Chalcogenide Letters*, vol. 11, no. 11, pp. 1-8, 2014.

[61] M. F. Faznny, M. K. Halimah, and M. N. Azlan, "Effect of lanthanum oxide on optical properties of zinc borotellurite glass system," *Journal of Optoelectronics and Biomedical Materials*, vol. 8, no. 2, pp. 49–59, 2016.

[62] H. M. Oo, H. Mohamed-Kamari, and W. M. D. Wan-Yusoff, "Optical Properties of Bismuth Tellurite Based Glass," *International Journal of Molecular Sciences*, vol. 13, no. 4, pp. 4623–4631, Apr. 2012, doi:10.3390/ijms13044623.

[63] M. N. Azlan, M. K. Halimah, S. Z. Shafinas, and W. M. Daud, "Polarizability and optical basicity of Er^{3+} ions doped tellurite based glasses," *Chalcogenide Letters*, vol. 11, no. 7, pp. 319, 2014.

[64] M. K. Halimah and C. Eevon, "Comprehensive study on the effect of Gd2O3 NPs on elastic properties of zinc borotellurite glass system using non-destructive ultrasonic technique," *Journal of Non-Crystalline Solids*, vol. 511, pp. 10–18, May 2019, doi:10.1016/j.jnoncrysol.2019.01.033.

[65] M. K. Halimah, A. A. Awshah, A. M. Hamza, K. T. Chan, S. A. Umar, and S. H. Alazoumi, "Effect of neodymium nanoparticles on optical properties of zinc tellurite glass system," *Journal of Materials Science: Materials in Electronics*, vol. 31, no. 5, pp. 3785–3794, Jan. 2020, doi: 10.1007/s10854-020-02907-9.